ACS APPLIED MATERIALS & INTERFACES

Research Article

www.acsami.org

Modified Two-Step Deposition Method for High-Efficiency TiO_2/$CH_3NH_3PbI_3$ Heterojunction Solar Cells

Jiangjian Shi, Yanhong Luo, Huiyun Wei, Jianheng Luo, Juan Dong, Songtao Lv, Junyan Xiao, Yuzhuan Xu, Lifeng Zhu, Xin Xu, Huijue Wu, Dongmei Li, and Qingbo Meng*

Key Laboratory for Renewable Energy and Beijing Key Laboratory for New Energy Materials and Devices, Institute of Physics, Chinese Academy of Sciences, Beijing 100190, P. R. China

Supporting Information

ABSTRACT: Hybrid organic−inorganic perovskites (e.g., $CH_3NH_3PbI_3$) are promising light absorbers for the third-generation photovoltaics. Herein we demonstrate a modified two-step deposition method to fabricate a uniform $CH_3NH_3PbI_3$ capping layer with high-coverage and thickness of 300 nm on top of the mesoporous TiO_2. The $CH_3NH_3PbI_3$ layer shows high light-harvesting efficiency and long carrier lifetime over 50 ns. On the basis of the as-prepared film, TiO_2/$CH_3NH_3PbI_3$ heterojunction solar cells achieve a power conversion efficiency of 10.47% with a high open-circuit voltage of 948 mV, the highest recorded to date for hole-transport-material-free (HTM-free) perovskite-based heterojunction cells. The efficiency exceeding 10% shows promising prospects for the HTM-free solar cells based on organic lead halides.

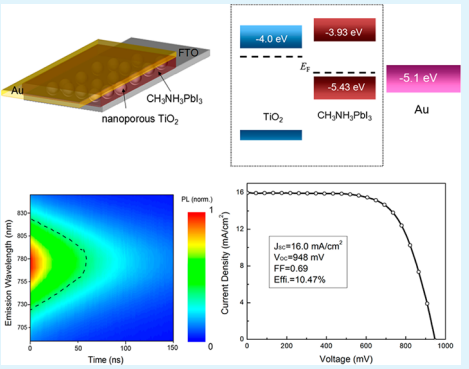

KEYWORDS: *organic lead iodide, hole-transport-material-free, heterojunction solar cell, modified two-step deposition method*

1. INTRODUCTION

Perovskite organic lead halides [e.g., $CH_3NH_3PbX_3$ (X = I, Br, Cl)] have attracted much attention in the past few years as light absorbers for thin film solar cells.[1,2] Together with iodide liquid electrolyte, $CH_3NH_3PbI_3$ and $CH_3NH_3PbBr_3$ were first employed to fabricate sensitized solar cells,[3] and a power conversion efficiency (PCE) beyond 6% was obtained with efforts.[4] The evolution of the cell from liquid state to solid state was achieved when organic polymers and molecules were introduced as hole transport materials (HTM) to substitute for the liquid iodide electrolyte. A PCE exceeding 9% was first realized when Spiro-OMeTAD was applied as HTM,[5] and the PCE was improved with optimization on the deposition conditions of perovskite absorbers. More recently, with two-step solution deposition or vacuum evaporation methods, impressive PCEs of over 15% have been achieved recently.[6,7]

However, most of the highly efficient perovskite-based solar cells used expensive organic molecules such as Spiro-OMeTAD as HTM, which increases the devices cost to a certain extent.[8,9] In fact, organic metal halides can act as not only light absorber but also excellent hole conductor.[10,11] Therefore, it is worth developing HTM-free solar cells through simplifying the manufacture process and improving their performance as much as possible. Until now, a few works have been focused on HTM-free solar cells with $CH_3NH_3PbI_3$ as the absorber layer,[12−14] and a PCE of 8% was achieved by Laban and and Etgar.[13] Recently, a PCE of the cell beyond 10% has been achieved in our group and the junction property of the HTM-free cell has been analyzed in detail with the diode model,[15] which confirmed the heterojunction nature of the cell.

In depositing the $CH_3NH_3PbI_3$ film for the solar cell, two solution methods have been developed: one-step spin-coating[3,5] and two-step deposition.[6,16,17] For the one-step spin-coating method, raw materials (PbI_2 and CH_3NH_3I) are mixed and dissolved in a suitable solvent as one precursor solution.[3] It is the most widely used method to prepare the solar cells, but it is difficult to control film properties such as thickness, uniformity, and morphology.[6,17] Even though Laban and Etgar demonstrated that the $CH_3NH_3PbI_3$ absorber layer with large crystals has been deposited with sequential spin-coating of the precursor solutions with different solvents, the highest PCE of 8% is still lower compared to the solar cells with HTM.[13] The two-step approach has been considered as a good method to fabricate $CH_3NH_3PbI_3$ films with high light absorption and controllable surface morphology.[6,17] To date, the two-step deposition method has only been applied in the HTM-based cells. In order to avoid PbI_2 crystals protruding from the surface of the mesoporous TiO_2 layer for a complete and fast conversion from PbI_2 to $CH_3NH_3PbI_3$, the spin-coating step of PbI_2 usually uses high spin speed[6] or low-concentration PbI_2 solution.[17] The HTM layer acts as an electron-blocking layer and also achieves a smooth film surface at the same time. Without the HTM layer, a new metal−

Received: April 8, 2014
Accepted: May 15, 2014
Published: May 15, 2014

semiconductor interface appears, and a good back contact is needed for high efficiency. Thus, more efforts need to be made to achieve a thick and uniform perovskite film with a smooth surface on mesoporous TiO_2 to avoid a short circuit arising from the direct contact between TiO_2 and the Au electrode and to ensure a good back-contact to the Au electrode. We found that a uniform, high-coverage $CH_3NH_3PbI_3$ perovskite film with a thick overlayer can hardly be deposited with the published two-step method.[6] Therefore, a more suitable film deposition method is needed to be developed for the HTM-free cells, especially for a good back-contact interface.

Herein, we report a modified two-step deposition (MTSD) method to fabricate the HTM-free perovskite solar cell. This method can be easily applied in the ambient condition and has no strict demands on deposition temperature. A uniform, high-coverage $CH_3NH_3PbI_3$ capping layer with high light absorption on the top of the mesoporous TiO_2 and a PCE of 10.47% have been realized with this method (Figure 1). The cells fabricated

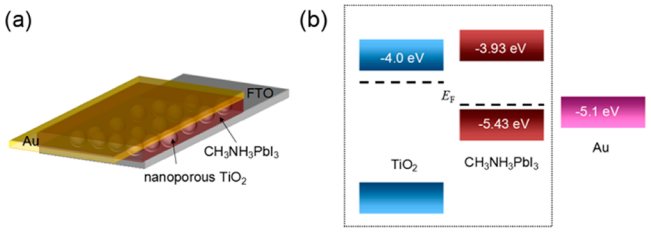

Figure 1. (a) Structure scheme and (b) energy level alignment of the $TiO_2/CH_3NH_3PbI_3$/Au heterojunction solar cell, where dash lines depict the Fermi energy level.

with this method all show high open-circuit voltages (V_{OC}) with an average value over 850 mV, and the highest V_{OC} is about 948 mV. In addition, impedance spectra (IS) were applied to further investigate the cell properties. Ideality factor and inverse saturated current densities of the cell have been obtained with the IS measurements to confirm the good heterojunction properties of the cell.

2. EXPERIMENTAL SECTION

2.1. Materials. PbI_2 and *N*,*N*-dimethylformide (DMF) were purchased from Sigma-Aldrich and Alfa Aesar, respectively. All the chemicals were directly used without further purification. Substrates of the cells are fluorine-doped tin oxide conducting glass (FTO) (Pilkington; thickness 2.2 mm, sheet resistance 14 Ω/square). CH_3NH_3I was synthesized by the literature method.[5] TiO_2 nanoparticles were synthesized with the hydrothermal method with a particle size of about 20 nm.

2.2. Cell Fabrication. All the experiments were carried out under ambient conditions with a humidity of about 20% at room temperature. First, a dense TiO_2 underlayer with a thickness of about 40 nm was spin coated onto the precleaned, laser-patterned FTO glass, which was then sintered at 500 °C for 30 min. A TiO_2 mesoporous layer with a thickness of 450 nm was deposited onto the underlayer with a screen printing method and sintered at 450 °C for 30 min. After that, TiO_2 films were treated with 25 mM $TiCl_4$ solution at 70 °C for 40 min and sintered at 500 °C for 30 min.

The $CH_3NH_3PbI_3$ absorber layer was deposited by the MTSD method. First, 1.2 M PbI_2 dissolved in DMF was spin-coated onto the TiO_2 film at a speed of 2000 rpm for 60 s and then heat treated at 90 °C for 2 min to remove the DMF solvent. After cooling to room temperature, the film was spin-coated with the 1.2 M PbI_2 in DMF for a second time to get a relatively thick and smooth film. After being spin-coated, PbI_2 films were heat-treated at 90 °C for another 2 min before being dipped into 10 mg/mL CH_3NH_3I solution with 2-propanol as the solvent. The total dipping time for PbI_2 films in CH_3NH_3I solutions is 120 min. After the dipping procedure, the $CH_3NH_3PbI_3$ absorber layer was obtained. After being thoroughly rinsed with 2-propanol, the obtained $CH_3NH_3PbI_3$ films were then heated at 90 °C for 45 min in air on a hot plate. After heat treatment, the films were kept in the dark in air overnight. Finally, Au was thermally evaporated (Kurt J. Lesker Co.) as electrode (80 nm) for heterojunction solar cells at an atmospheric pressure of 10^{-7} Torr for work functions matching.[18]

2.3. Characterization of the Solar Cell. Current−voltage (I−V) characteristics were measured by an additional voltage from the 2602 system source meter of Keithley together with a sunlight simulator (Oriel Solar Simulator 91192, AM 1.5100 mW/cm^2) calibrated with a standard silicon reference cell. The solar cells were masked with a black aperture to define the active area of 0.08 cm^2 and measured in a lab-made light-tight sample holder. Monochromatic incident photon-to-electron conversion efficiency (IPCE) was measured with a lab-made IPCE spectrometer[19,20] with wavelength ranging from 350 to

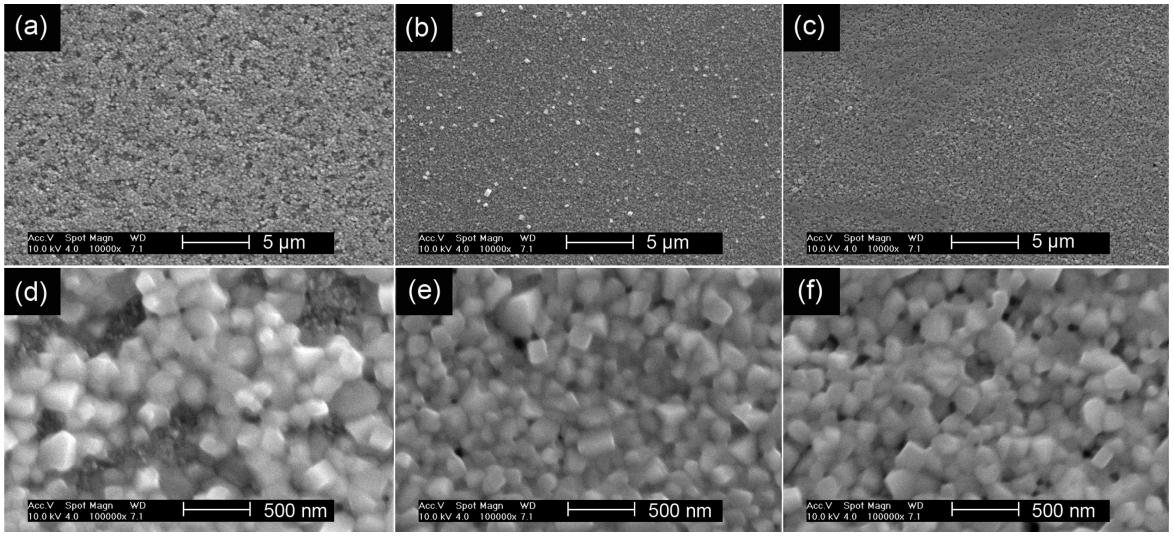

Figure 2. Top view scanning electron microscopy images of $CH_3NH_3PbI_3$ films on TiO_2 mesoporous films. The PbI_2 was spin-coated one (a, d), two (b, e), and three (c, f) times, respectively.

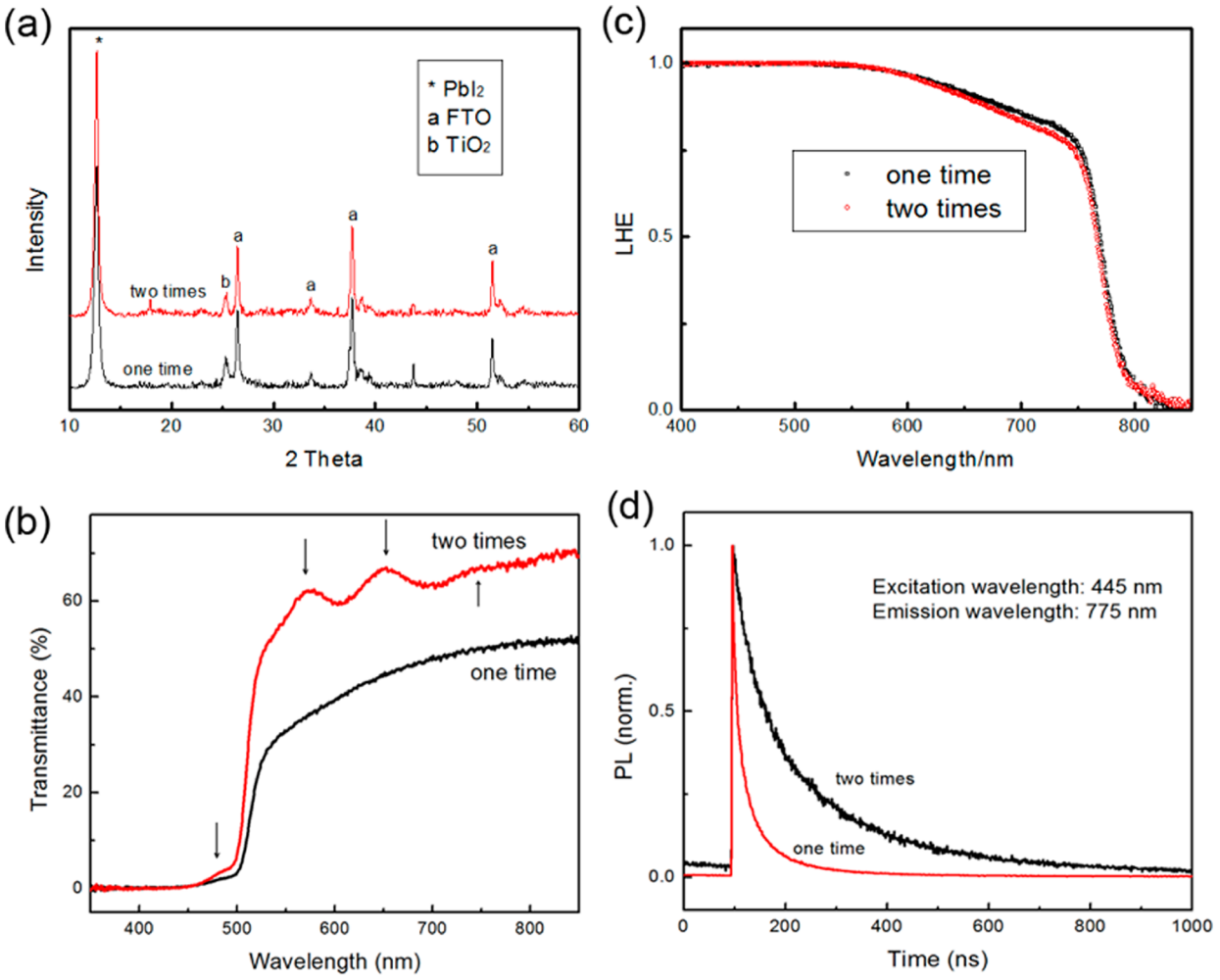

Figure 3. X-ray diffraction (a) and transmittance spectra (c) of the PbI_2 films spin-coated one and two times, and light absorption efficiency (LHE) (b) and transient photoluminescence (PL) spectra (d) of the corresponding $CH_3NH_3PbI_3$ films.

850 nm. Scanning electron microscopy (SEM) images were obtained with an FEI-SEM (XL 30 S-FEG). UV−vis absorption and transmittance spectrum was measured with UV−vis spectrophotometer (UV-2550, Shimadzu) with wavelength ranging from 350 to 850 nm. Impedance spectra were measured with an IM6ex electrochemical workstation with a sunlight simulator of 100 mW/cm^2 (AM 1.5). The scanning frequency was set between 100 kHz and 100 mHz and the amplitude of the sine perturbation bias was 10 mV. Different dc positive bias was also applied when measuring. X-ray diffraction (XRD) was measured with a Bruker X-ray diffractometer with Cu Kα as the radiation source. The steady-state photoluminescence (PL) spectra were measured using the PL spectrometer (Edinburgh Instruments, FLS 900) with xenon as the excitation source. The detected emission wavelength of the steady-state PL is from 650 to 850 nm. The transient PL spectra were measured with the same instrument together with a pulsed diode laser (EPL-445, 0.8 μJ/cm^2) at a pulse frequency of 1 MHz. An optical filter at 590 nm was used to filter out the excitation light both in steady-state and transient PL measurements.

3. RESULTS AND DISCUSSIONS

The two-step deposition method was first employed by Grätzel and co-workers for depositing the $CH_3NH_3PbI_3$ absorber layer in perovskite solar cells with Spiro-OMeTAD as HTM. A high spin-coating speed of 6500 rpm or PbI_2 solution with low concentration (0.4 M) was used to ensure depositing the PbI_2 infiltrating in the mesoporous TiO_2 but not forming a overlayer.[6,17] For HTM-free cells, the perovskite absorber on the mesoporous TiO_2 should have an appropriate thickness to avoid forming shunt pathways.[13,21] Therefore, a relatively low spin speed of 2000 rpm and high concentrated PbI_2 solutions (1.2 M) were used to spin-coat the PbI_2 layer in our work. Although the PCE of the cell can be promoted by slowing down the spin-coating speed and increasing the concentration of PbI_2 solution, a uniform and full coverage of $CH_3NH_3PbI_3$ crystals on TiO_2 films cannot be obtained with spin-coating the PbI_2 once, as seen in Figure 2a,d. Further investigation found that the incomplete coverage on the TiO_2 film with $CH_3NH_3PbI_3$ crystals is mainly attributed to the relatively rough surface of the prepared PbI_2 films (Figure S1a, Supporting Information), since the morphology of $CH_3NH_3PbI_3$ absorber layer is mainly determined by the PbI_2 film.[22] Interestingly, by spin-coating the PbI_2 solution for a second time, the morphology of the PbI_2 film on TiO_2 are ameliorated obviously and a complete coverage of $CH_3NH_3PbI_3$ on TiO_2 film with interconnected crystals can be obtained, as seen in Figure S1b,e (Supporting Information). However, why the repeated spin-coating of PbI_2 solutions can ameliorate the surface morphology is still unclear, and no obvious difference in the crystallization can be observed with the XRD results, as shown in Figure 3a. Possible reasons contributing to such a phenomenon could be the crystal-

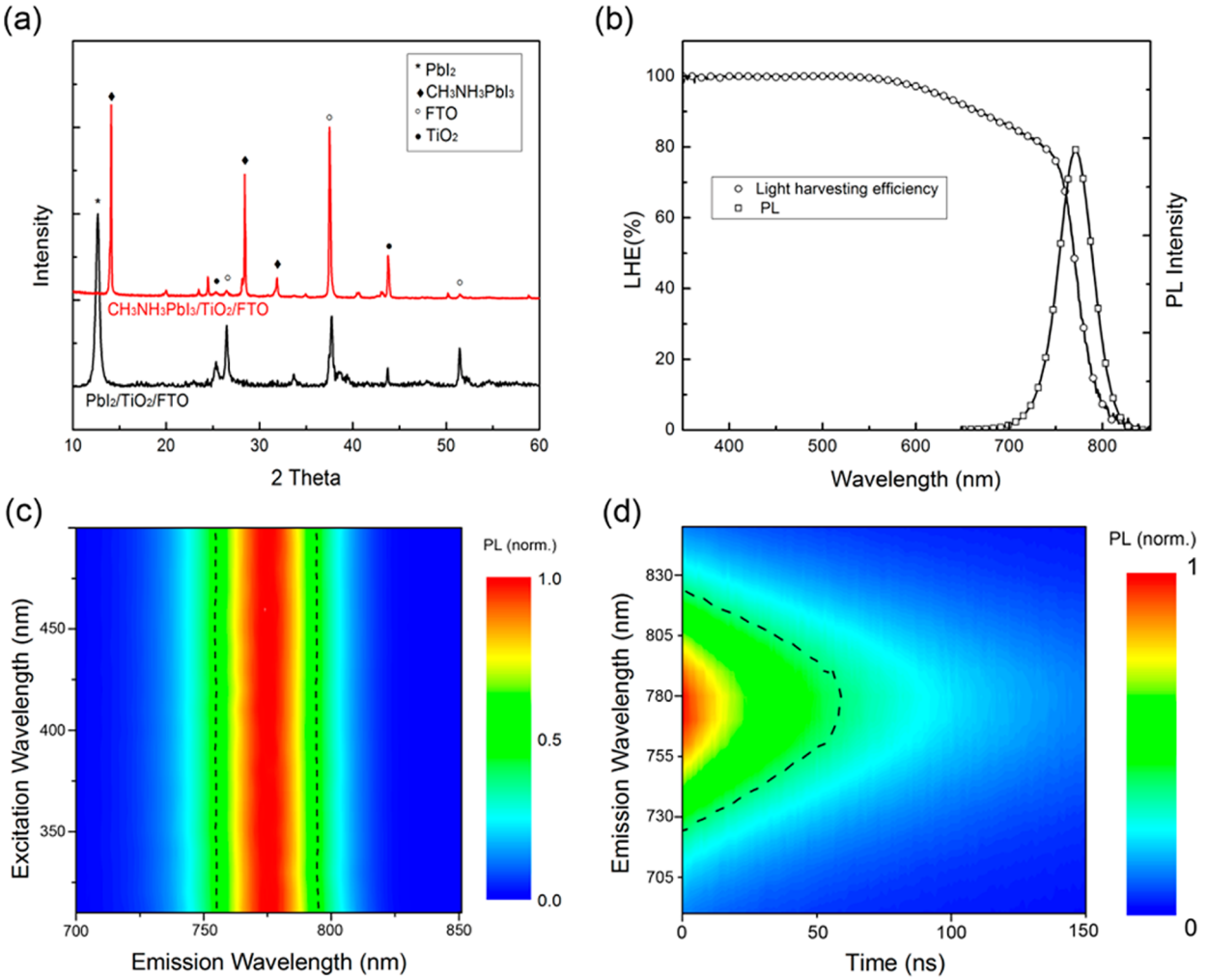

Figure 4. (a) X-ray diffraction for PbI_2 and $CH_3NH_3PbI_3$ films, (b) light-harvesting efficiency (LHE) and steady-state photoluminescence (PL) spectrum (excited at 525 nm) of the $CH_3NH_3PbI_3$ film, (c) steady-state PL spectrum induced by light with varied wavelengths (300−500 nm), and (d) transient PL spectrum at varied emission wavelengths excited by a pulsed diode laser at 445 nm.

lization−dissolving−recrystallization process and an amelioration of the surface wetting, which allow the highly concentrated PbI_2 solution to cover the TiO_2 mesoporous film uniformly. The difference in the surface morphology has an obvious influence on the light transmittance properties of the films. As in Figure 3b, the transmittance of the PbI_2 film spin-coated one time is much lower than that spin-coated two times, which is mainly attributed to the scattering from the rough surface. Meanwhile, the optical interference peaks (marked as arrows in Figure 3b) of the PbI_2 film can be observed in the transmittance spectrum when spin-coating two times, which further confirms the uniformity of the film deposited with the MTSD method. It has to be noted that, despite the different times the PbI_2 was spin-coated, no obvious difference in the light-harvesting efficiency (LHE) of the $CH_3NH_3PbI_3$ films has been observed (Figure 3c). Figure 3d shows the transient PL spectra of the $CH_3NH_3PbI_3$ films spin-coated with PbI_2 once or twice. It is worth noting that the PL lifetime of $CH_3NH_3PbI_3$ has been prolonged significantly with the MTSD method, which can be attributed to the uniformity of the absorber layer with fewer defects.[18] However, spin-coating more than two times cannot make further improvement of the coverage and surface morphology, as seen in Figure S1c,f (Supporting Information). Thus, all the following work was carried out by spin-coating the PbI_2 twice.

With the immersion procedure, the $CH_3NH_3PbI_3$ absorber layer is obtained. Figure 4a gives the XRD results of the $CH_3NH_3PbI_3$ as well as the PbI_2 films. The PbI_2 prepared by spin-coating grows in a preferential orientation along its *c* axis.[6] From the XRD of $CH_3NH_3PbI_3$ film, it can be found that all the PbI_2 has been converted into $CH_3NH_3PbI_3$ with the immersion procedure. A set of strong sharp diffraction peaks at 14.09°, 28.43°, and 31.87° corresponding to the (110), (220), and (310) crystal planes of $CH_3NH_3PbI_3$ appears, indicating good crystallization. Figure 4b gives the LHE as well as the steady-state PL spectrum of the $CH_3NH_3PbI_3$ film prepared with the MTSD method mentioned above. From the LHE, it can be found that most of the incident light is absorbed by the $CH_3NH_3PbI_3$ layer. Meanwhile, the LHE in the long-wavelength range is also very high, benefiting from low light loss due to incomplete light absorption. The PL spectrum shows a smooth peak at the onset of the LHE spectrum with an fwhm of about 50 nm, indicating that most of the photoinduced carriers are accumulating in the band edges and light through direct recombination.[18] With the LHE and PL spectrum, the band gap width of the absorber can be estimated to be 1.61 eV, a little larger than that of the bulk $CH_3NH_3PbI_3$,[23] a typical

dx.doi.org/10.1021/am502131t | ACS Appl. Mater. Interfaces 2014, 6, 9711−9718

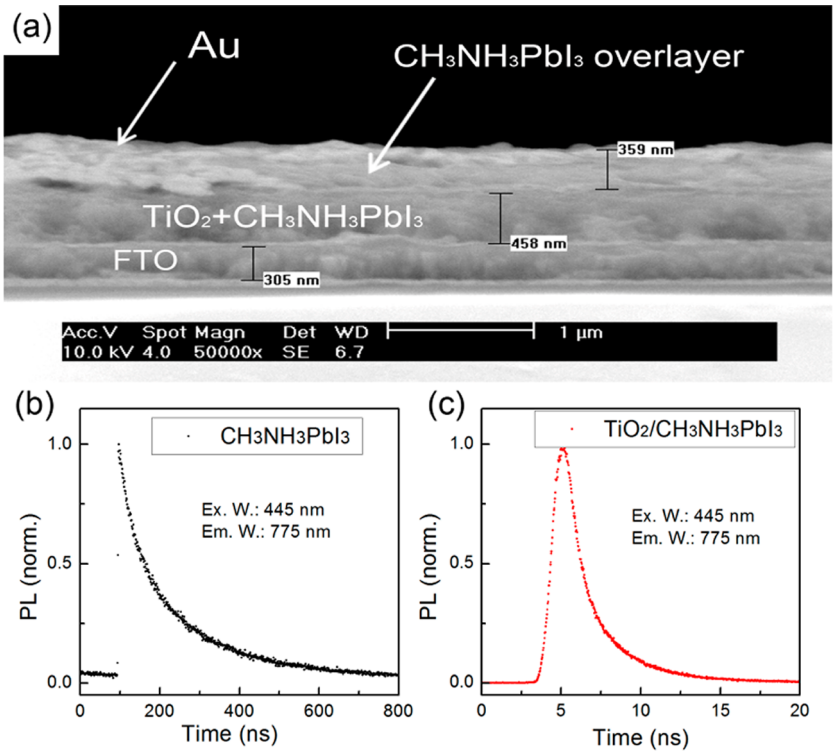

Figure 5. (a) Cross-sectional scanning electron microscopy (SEM) image of the HTM-free solar cell, and transient photoluminescence (PL) spectra of $CH_3NH_3PbI_3$ films (b) without and (c) with the mesoporous TiO_2 involved.

feature for $CH_3NH_3PbI_3$ deposited in the mesoporous TiO_2 scaffold structure.[23] Figure 4c gives the steady-state PL spectrum excited by varied wavelength (300−500 nm). It is obvious that the peaks of all the PL spectra are at the same wavelength of about 775 nm. In a photon−electron interaction process, the electrons are always excited in a direct-transition way by absorbing the whole energy of a photon. Calculations find that more than one directly opposite band edge with different width exist in the energy band structure of $CH_3NH_3PbI_3$,[10] which means that several direct excitation and emission pathways exist in this material. However, all the excitation lights with varied wavelengths can induce PL at 775 nm, which indicates that the photoinduced carriers can transfer to the conduction band minimum (CBM) and valence band maximum (VBM) by fast relaxation.[24] It is of importance for carriers transferring to the CBM and VBM by fast relaxation to obtain a small effective mass when transporting in the semiconductor.[10] Figure 4d gives the transient PL spectra at varied emission wavelengths excited by a pulsed diode laser at 445 nm. The peak wavelength of the PL is also at 775 nm with the strongest intensity. The dash line in Figure 4d depicts the contour of the PL intensity of $1/e$,[25] and the effective lifetime of the carriers in the CBM and VBM can be deduced to be over 50 ns, longer than what has been reported.[24,25] The relatively long carrier lifetime indicates that the $CH_3NH_3PbI_3$ crystals prepared with the MTSD method have good quality with few body or interface defects for recombination. As is known, a long carrier lifetime is needed to achieve a long diffusion length and thus to achieve a high carrier collection efficiency. With the diffusion constant of $CH_3NH_3PbI_3$, the carrier diffusion length of the absorber layer in our cell is more than 200 nm.[25] Meanwhile, no PL peak transition has been observed with the evolution of time at the nanosecond scale, which means that the carrier relaxation in the energy space is ultrafast.[24]

Figure 5a gives the cross sectional SEM image of the cell. The TiO_2 mesoporous layer infiltrated with $CH_3NH_3PbI_3$ with a thickness of 450 nm as well as a 280-nm-thick $CH_3NH_3PbI_3$ capping layer can be observed. The transient PL spectra of $CH_3NH_3PbI_3$ at 775 nm without and with the TiO_2 are given in parts b and c of Figure 5, respectively. It is obvious that when the TiO_2 was involved, the PL of $CH_3NH_3PbI_3$ was quickly quenched, which indicates that the photoinduced free electrons in $CH_3NH_3PbI_3$ can be quickly extracted by the TiO_2. With the MTSD method, a series of efficient HTM-free solar cells have been fabricated. The $I-V$ curve of the best-performing cell is shown in Figure 6a. The PCE of the cell is 10.47% with a short-circuit current density (J_{SC}) of 16.0 mA/cm^2, V_{OC} of 948 mV, and fill factor (FF) of 0.69. It is worth noting that the V_{OC} of the cell is unexpectedly high[12−14] and is comparable to that of the cell with Spiro-OMeTAD [5], although the J_{SC} is lower than for those cells. In a heterojunction or a p-i-n solar cell, the V_{OC} is mainly determined by the difference in Fermi energy levels of n-type and p-type semiconductors.[18] Experiments find that a high density of free holes exists in the perovskite organic metal halide compounds,[13] which means that the Fermi energy level of such compounds is low.[18] The VBM of $CH_3NH_3PbI_3$ is about −5.43 eV and the highest occupied molecular orbital (HOMO) of Spiro-OMeTAD is about −5.22 eV [5]. The Fermi energy level of the p-type $CH_3NH_3PbI_3$ can be calculated with the equation[18]

$$E_F = E_i - k_B T \ln\left(\frac{N_A}{n_i}\right) \quad (1)$$

where E_i is the intrinsic energy level of a semiconductor, which is usually in the middle of band gap, N_A is the free hole density, n_i is the intrinsic carrier density, k_B is the Boltzmann constant, and T is the absolute temperature. With the effective mass of

dx.doi.org/10.1021/am502131t | ACS Appl. Mater. Interfaces 2014, 6, 9711−9718

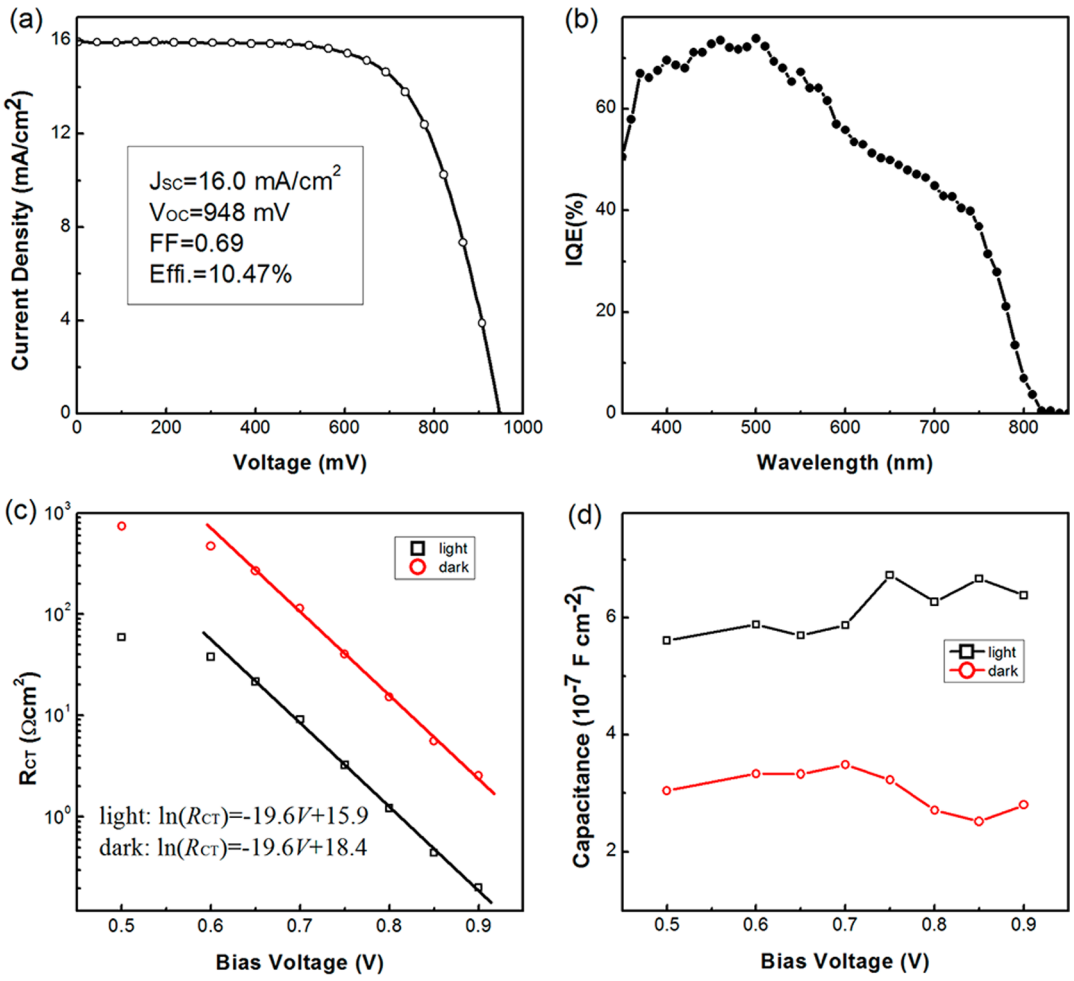

Figure 6. (a) Current−voltage curve and (b) the internal quantum efficiency of the best-performing cell and (c) charge transfer resistance and (d) capacitance properties of the cell under illumination (AM 1.5, 100 mW/cm^2) and in the dark.

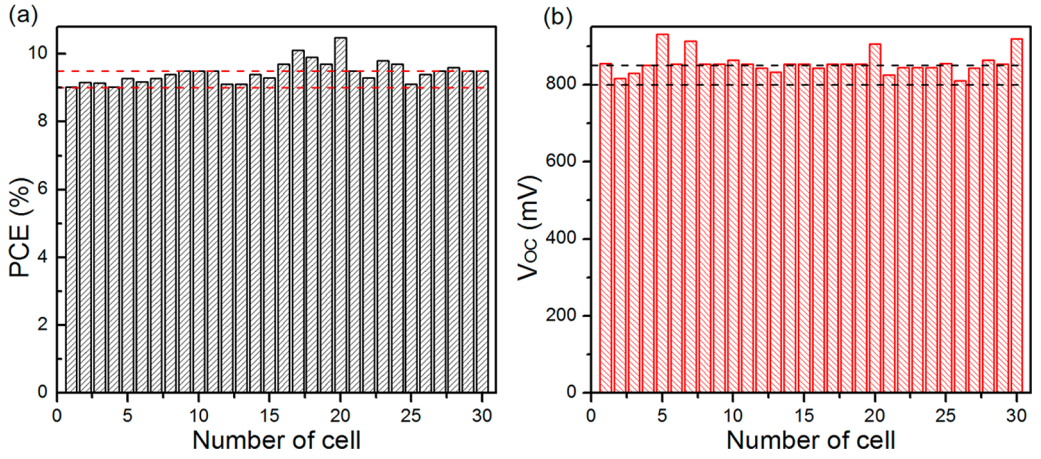

Figure 7. Histogram of (a) power conversion efficiency (PCE) and (b) open-circuit voltage (V_{OC}) of 30 cells.

the electron and hole in $CH_3NH_3PbI_3$, the n_i is calculated to be 10^6 cm^{-3}.[10,18] Further with the N_A of about 10^{17} cm^{-3} from Laban and Etgar's report,[13] the E_F can be calculated to be −5.34 eV, even lower than the HOMO energy level of Spiro-OMeTAD (Figure 1b), which means that the V_{OC} of the TiO_2/$CH_3NH_3PbI_3$/Au heterojunction solar cell can even be higher than that of the cell with HTM. However, it still has to be pointed out that the Fermi energy level of $CH_3NH_3PbI_3$ is also lower than that of the Au electrode, leading to an energy barrier of about 0.24 eV as well as a depleted region of over 60 nm existing in the back-contact region.[18] Such a barrier does harm to the transportation of free carriers in the back-contact region, thus leading to a decrease in the internal quantum efficiency (IQE) in the long-wavelength region,[14] as shown in Figure 6b. Interestingly, the V_{OC} of our result is also much higher than Etgar et al.'s recent-published result (840 mV),[26] which can be

dx.doi.org/10.1021/am502131t | ACS Appl. Mater. Interfaces 2014, 6, 9711−9718

attributed to experimental differences in film thickness of the TiO_2 mesoporous layer and the dipping procedure.

To further clarify the property of the cell, impedance spectrum measurements were carried out. The charge recombination resistance (R_{CT}) and the capacitance (C) are derived from the Nyquist plots with an RC element as the equivalent circuit in the intermediate frequency region (Figure S2, Supporting Information).[27] With the ideal model for a single heterojunction solar cell, the R_{CT} of the cell can be deduced as[9,15,28]

$$R_{CT} = \frac{Ak_BT}{eJ_0} \exp\left(-\frac{eV}{Ak_BT}\right) \quad (2)$$

where A is the ideality factor of a heterojunction solar cell (in the range $1 < A < 2$), e is the elementary charge, J_0 is the inverse saturated current density of a heterojunction, and V is the bias voltage. With the fitting results according to eq 2 in Figure 6c, the ideality factor under both illumination and in the dark is derived as $A = 1.97$. The value of the ideality factor close to 2 indicates that the J_0 of the cell is dominated by the carrier recombination through trap states in the space charge region of TiO_2 and $CH_3NH_3PbI_3$,[15,28] confirming the junction nature of the HTM-free solar cell, consistent with the results in the literature.[13,15] Meanwhile, the J_0 can be calculated to be 5.76×10^{-6} and 5.23×10^{-7} mA/cm^2 when under illumination and in the dark, respectively. The J_0 is relatively small, which is comparable to that of the high-efficiency $Cu(In,Ga)Se_2$ and $Cu_2ZnSn(S,Se)_4$ solar cells,[28,29] which is beneficial for achieving high V_{OC}, FF, and PCE. As in Figure 6d, the capacitance under illumination is somewhat larger than that in the dark, which is mainly attributed to the high density of carriers in $CH_3NH_3PbI_3$ induced by light.[30] The high density of free carriers would increase the recombination current of the cell,[18] consistent with the values of J_0 calculated above.

Figure 7 gives the histogram plots of PCE and V_{OC} of 30 efficient heterojunction cells. It can be found that the PCEs of the cells are all exceeding 9.0% and the average PCE is over 9.4%. Meanwhile, all the V_{OC}s are larger than 800 mV, with an average value over 850 mV. The histogram demonstrates the reproductivity of the cell fabricated with the MTSD method and thevpromising prospects of the cell without expensive HTMs. However, the J_{SC} is still lower than that of the cell with Spiro-OMeTAD, which is mainly attributed to the relatively low IQE, especially in the long-wavelength range. Interface recombination and carrier transport barriers in the cell can be the main reasons for the low IQE, since the carrier collection field is weaker than that of p-i-n solar cells.[14] To further improve the performance of the cell, deposition methods for high-quality absorber and interface engineering should be developed, and a more lucid insight into the cell is also needed.

In conclusion, the two-step deposition method is modified to achieve a uniform and high-coverage perovskite absorber layer with a long carrier lifetime. A mesoporous $TiO_2/CH_3NH_3PbI_3$ HTM-free heterojunction cell with a high efficiency of 10.47% as well as a high V_{OC} of 948 mV has been fabricated with this MTSD method. Further calculation reveals that the Fermi energy of $CH_3NH_3PbI_3$ is about −5.34 eV, even lower than the HOMO energy level of Spiro-OMeTAD, which explains the high V_{OC} of the cell. Investigation based on the impedance spectrum measurements indicates that the cell in this work is a typical heterojunction solar cell with an ideality factor of 1.97 and recombination current densities comparable to that of the high-efficiency heterojunction solar cells. The high efficiency and reproductivity of the cell with the MTSD method demonstrate the promising prospects of the HTM-free solar cells. Further efforts will be made to increase the carrier collection efficiency, thus increasing the performance of the cell in the following work. We believe that the performance of the cell can be further improved if more investigations are made on materials and interfaces.

■ ASSOCIATED CONTENT

Supporting Information

Optical microscope image of the PbI_2 films, SEM images of $CH_3NH_3PbI_3$, and Nyquist as well as the Bode plots from the impedance spectrum measurements. This material is available free of charge via the Internet http://pubs.acs.org.

■ AUTHOR INFORMATION

Corresponding Author

*E-mail: qbmeng@iphy.ac.cn.

Notes

The authors declare no competing financial interests.

■ ACKNOWLEDGMENTS

This work was supported by Beijing Science and Technology Committee (Z131100006013003), National Key Basic Research Program (No. 2012CB932903), and Natural Science Foundation of China (Nos. 21173260 and 91233202).

■ REFERENCES

(1) Park, N. G. Organometal Perovskite Light Absorbers toward a 20% Efficiency Low-Cost Solid-State Mesoscopic Solar Cell. *J. Phys. Chem. Lett.* **2013**, *4*, 2423−2429.

(2) Snaith, H. J. Perovskites: The Emergence of a New Era for Low-Cost, High-Efficiency Solar Cells. *J. Phys. Chem. Lett.* **2013**, *4*, 3623−3630.

(3) Kojima, A.; Teshima, K.; Shirai, Y.; Miyasaka, T. Organometal Halide Perovskites as Visible-Light Sensitizers for Photovoltaic Cells. *J. Am. Chem. Soc.* **2009**, *131*, 6050−6051.

(4) Im, J. H.; Lee, C. R.; Lee, J. W.; Park, S. W.; Park, N. G. 6.5% Efficient Perovskite Quantum-Dot-Sensitized Solar Cell. *Nanoscale* **2011**, *3*, 4088−4093.

(5) Kim, H. S.; Lee, C. R.; Im, J. H.; Lee, K. B.; Moehl, T.; Marchioro, A.; Moon, S. J.; Baker, R. H.; Yum, J. H.; Moser, J. E.; Grätzel, M.; Park, N. G. Lead Iodide Perovskite Sensitized All-Solid-State Submicron Thin Film Mesoscopic Solar Cell with Efficiency Exceeding 9%. *Sci. Rep.* **2012**, *2*, 591−597.

(6) Burschka, J.; Pellet, N.; Moon, S. J.; Baker, R. H.; Gao, P.; Nazeeruddin, M. K.; Grätzel, M. Sequential Deposition as a Route to High-Performance Perovskite-Sensitized Solar Cells. *Nature* **2013**, *499*, 316−319.

(7) Liu, M.; M. Johnston, B.; Snaith, H. J. Efficient Planar Heterojunction Perovskite Solar Cells by Vapour Deposition. *Nature* **2013**, *501*, 395−398.

(8) Jeon, N. J.; Lee, J.; Noh, J. H.; Nazeeruddin, M. K.; Gratzel, M.; Il Seok, S. Efficient Inorganic−Organic Hybrid Perovskite Solar Cells Based on Pyrene Arylamine Derivatives as Hole-Transporting Materials. *J. Am. Chem. Soc.* **2013**, *135*, 19087−19090.

(9) Christians, J. A.; Fung, R. C. M.; Kamat, P. V. An Inorganic Hole Conductor for Organo-Lead Halide Perovskite Solar Cells. Improved Hole Conductivity with Copper Iodide. *J. Am. Chem. Soc.* **2014**, *136*, 758−764.

(10) Giorgi, G.; Fujisawa, J. I.; Segawa, H.; Yamashita, K. Small Photo Carrier Effective Masses Featuring Ambipolar Transport in Methylammonium Lead Iodide Perovskite: A Density Function Analysis. *J. Phys. Chem. Lett.* **2013**, *4*, 4213−4216.

(11) Chung, In; Song, J.-H.; Im, J.; Androulakis, J.; Malliakas, C. D.; Li, H.; Freeman, A. J.; Kenney, J. T.; Kanatzidis, M. G. $CsSnI_3$: Semiconductor or Metal? High Electrical Conductivity and Strong Near-Infrared Photoluminescence from a Single Material. High Hole Mobility and Phase-Transitions. *J. Am. Chem. Soc.* **2012**, *134*, 8579−8587.
(12) Etgar, L.; Gao, P.; Xue, Z.; Peng, Q.; Chandiran, A. K.; Liu, B.; Nazeeruddin, Md. K.; Grätzel, M. Mesoscopic $CH_3NH_3PbI_3/TiO_2$ Heterojunction Solar Cells. *J. Am. Chem. Soc.* **2012**, *134*, 17396−17399.
(13) Laban, W. A.; Etgar, L. Depleted Hole Conductor-Free Lead Halide Iodide Heterojunction Solar Cell. *Energy Environ. Sci.* **2013**, *6*, 3249−3253.
(14) Shi, J. J.; Dong, W.; Xu, Y. Z.; Li, C. H.; Lv, S. T.; Zhu, L. F.; Dong, J.; Luo, Y. H.; Li, D. M.; Meng, Q. B.; Chen, Q. Enhanced Performance in Perovskite Organic Lead Iodide Heterojunction Solar Cells with Metal−Insulator−Semiconductor Back Contact. *Chin. Phys. Lett.* **2013**, *30*, 128402.
(15) Shi, J. J.; Dong, J.; Lv, S. T.; Xu, Y. Z.; Zhu, L. F.; Xiao, J. Y.; Xu, X.; Wu, H. J.; Li, D. M.; Luo, Y. H.; Meng, Q. B. Hole-Conductor-Free Perovskite Organic Lead Iodide Heterojunction Thin-Film Solar Cells: High Efficiency and Junction Property. *Appl. Phys. Lett.* **2014**, *104*, 063901.
(16) Chen, Q.; Zhou, H. P.; Hong, Z. R.; Luo, S.; Duan, H. S.; Wang, H. H.; Liu, Y. S.; Li, G.; Yang, Y. Planar Heterojunction Perovskite Solar Cells via Vapor-Assisted Solution Process. *J. Am. Chem. Soc.* **2014**, *136*, 622−625.
(17) Bi, D.; Häggman, L.; Boschloo, G.; Yang, L.; Johansson, E. M. J.; Hagfeldt, A. Using Two-Step Deposition Technique To Prepare Perovskite ($CH_3NH_3PbI_3$) for Thin Film Solar Cells Based on ZrO_2 and TiO_2 Mesostructures. *RSC Adv.* **2013**, *3*, 18762−18766.
(18) Sze, S. M.; Ng, K. K. *Physics of Semiconductor Devices*, 3rd ed.; Wiley: New York, 2006.
(19) Guo, X. Z.; Luo, Y. H.; Zhang, Y. D.; Huang, X. C.; Li, D. M.; Meng, Q. B. Study on The Effect of Measuring Methods on Incident Photo-to-Electron Conversion Efficiency of Dye-Sensitized Solar Cells by Home-Made Setup. *Rev. Sci. Instrum.* **2010**, *81*, 103106.
(20) Guo, X. Z.; Luo, Y. H.; Li, C.; Qin, D.; Li, D. M.; Meng, Q. B. Can the Incident Photo-to-Electron Conversion Efficiency Be Used To Calculate Short-Circuit Current Density of Dye-Sensitized Solar Cells. *Curr. Appl. Phys.* **2012**, *12*, e54−e58.
(21) Eperon, G. E.; Burlakov, V. M.; Docampo, P.; Goriely, A.; Snaith, H. J. Morphological Control for High Performance, Solution-Processed Planar Heterojunction Perovskite Solar Cells. *Adv. Funct. Mater.* **2014**, *24*, 151−157.
(22) Liang, K.; Mitzi, D. B.; Prikas, M. T. Synthesis and Characterization of Organic−Inorganic Perovskite Thin Films Prepared Using a Versatile Two-Step Dipping Technique. *Chem. Mater.* **1998**, *10*, 403−411.
(23) Choi, J. J.; Yang, X.; Norman, Z. M.; Billinge, S. J. L.; Owen, J. S. Structure of Methylammonium Lead Iodide within Mesoporous Titanium Dioxide: Active Material in High-Performance Perovskite Solar Cells. *Nano Lett.* **2014**, *14*, 127−133.
(24) Xing, G.; Mathews, N.; Sun, S.; Lim, S. S.; Lam, Y. M.; Grätzel, M.; Mhaisalkar, S.; Sum, T. C. Long-Range Balanced Electron and Hole-Transport Lengths in Organic−Inorganic $CH_3NH_3PbI_3$. *Science* **2013**, *342*, 344−347.
(25) Stranks, S. D.; Eperon, G. E.; Grancini, G.; Menelaou, C.; Alcocer, M. J. P.; Leijtens, T.; Herz, L. M.; Petrozza, A.; Snaith, H. J. Electron-Hole Diffusion Lengths Exceeding 1 Micrometer in an Organometal Trihalide Perovskite Absorber. *Science* **2013**, *342*, 341−344.
(26) Aharon, S.; Gamliel, S.; Cohen, B. E.; Etgar, L. Depletion Region Effect of Highly Efficient Hole Conductor Free $CH_3NH_3PbI_3$ Perovskite Solar Cells. *Phys. Chem. Chem. Phys.* **2014**, *16*, 10512−10518.
(27) Dualeh, A.; Moehl, T.; Tétreault, N.; Teuscher, J.; Gao, P.; Nazeeruddin, M. K.; Grätzel, M. Impedance Spectroscopic Analysis of Lead-Iodide Perovskite-Sensitized Solid-State Solar Cells. *ACS Nano* **2014**, *8*, 362−373.
(28) Hegedus, S. S.; Shafarman, W. N. Thin-Film Solar Cells: Device Measurements and Analysis. *Prog. Photovolt.: Res. Appl.* **2004**, *12*, 155−176.
(29) Bag, S.; Gunawan, O.; Gokmen, T.; Zhu, Y.; Todorov, T. K.; Mitzi, D. B. Low Band Gap Liquid-Processed CZTSe Solar Cell with 10.1% Efficiency. *Energy Environ. Sci.* **2012**, *5*, 7060−7065.
(30) Kim, H.-S.; Mora-Sero, I.; Gonzalez-Pedro, V.; Fabregat-Santiago, F.; Juarez-Perez, E. J.; Park, N.-G.; Bisquert, J. Mechanism of Carrier Accumulation in Perovskite Thin-Absorber Solar Cells. *Nat. Commun.* **2013**, *4*, 2242.